

Detection of CH₃SH in protostar IRAS 16293-2422

L. Majumdar^{1,2,3*}, P. Gratier^{1,2}, T. Vidal^{1,2}, V. Wakelam^{1,2}, J.-C. Loison^{4,5},
K. M. Hickson^{4,5}, E. Caux^{6,7}

¹ *Univ. Bordeaux, LAB, UMR 5804, F-33270, Floirac, France.*

² *CNRS, LAB, UMR 5804, F-33270, Floirac, France*

³ *Indian Centre For Space Physics, 43 Chalantika, Garia Station Road, Kolkata, 700084, India*

⁴ *Univ. Bordeaux, ISM, UMR 5255, F-33400 Talence, France*

⁵ *CNRS, ISM, UMR 5255, F-33400 Talence, France*

⁶ *Université de Toulouse, UPS-OMP, IRAP, Toulouse, France*

⁷ *CNRS, IRAP, 9 Av. Colonel Roche, BP 44346, F-31028 Toulouse Cedex 4, France*

Accepted XXX. Received YYY; in original form ZZZ

ABSTRACT

The nature of the main sulphur reservoir in star forming regions is a long standing mystery. The observed abundance of sulphur-bearing species in dense clouds is only about 0.1 per cent of the same quantity in diffuse clouds. Therefore, the main sulphur species in star forming regions of the interstellar medium are still unknown. IRAS 16293-2422 is one of the regions where production of S-bearing species is favourable due to its conditions which allows the evaporation of ice mantles. We carried out observations in the 3 mm band towards the solar type protostar IRAS 16293-2422 with the IRAM 30m telescope. We observed a single frequency setup with the EMIR heterodyne 3 mm receiver with an Lower Inner (LI) tuning frequency of 89.98 GHz. Several lines of the complex sulphur species CH₃SH were detected. Observed abundances are compared with simulations using the NAUTILUS gas-grain chemical model. Modelling results suggest that CH₃SH has the constant abundance of 4×10^{-9} (compared to H₂) for radii lower than 200 AU and is mostly formed on the surfaces. Detection of CH₃SH indicates that there may be several new families of S-bearing molecules (which could form starting from CH₃SH) which have not been detected or looked for yet.

Key words: Astrochemistry, ISM: molecules, ISM: abundances, ISM: evolution, methods: statistical

1 INTRODUCTION

Though sulphur is only the tenth most abundant element in the interstellar medium (ISM) and stars, it has long been of interest for astrochemists. First of all, the reservoir of sulphur in dense regions is a matter of debate. The depletion of sulphur in the diffuse medium does not seem to occur as its atomic abundance in the gas-phase is rather constant with the line of sight (Sofia et al. 1994) even though these measurements are uncertain (Jenkins 2009). The observed abundance of sulphur-bearing species in dense interstellar media is still only a few percent of the cosmic reference (Tieftrunk et al. 1994; Wakelam et al. 2004a; Anderson et al. 2013). The most simple explanation is that atomic sulphur depletes on interstellar grains with increasing density and it is converted into H₂S on the surface (Charnley 1997). However, the lack of a solid H₂S feature in the original signature in ISO spectra of high (Gibb et al. 2000a) and low (Boogert et al. 2000)

mass protostars sets an upper limit on the mantle H₂S abundance which cannot exceed about 10^{-7} with respect to H₂ (van Dishoeck & Blake 1998). Other more or less refractory (polymers or aggregates of sulphur) have then been proposed as reservoirs for interstellar sulphur (Wakelam et al. 2004b; Druard & Wakelam 2012; Woods et al. 2015). Whatever its form, it is now acknowledged that sulphur is mostly present on grain surfaces in dense environment. In the envelopes of protostars, through thermal desorption, this sulphur returns to the gas-phase and produces a chemical chain forming first SO and then SO₂ (Charnley 1997; Buckle & Fuller 2003; Wakelam et al. 2004b). Assuming that part of the initial sulphur is in the form of H₂S and/or OCS, the relative abundance ratios of these four species could be in principle used as chemical clocks of high and low mass protostars (Hatchell et al. 1998; Wakelam et al. 2011; Li et al. 2015).

CS was the first sulphur bearing molecule detected in the interstellar medium (Penzias et al. 1971). Since then, several sulphur-bearing molecules have been detected in the interstellar medium and circumstellar shells in the Milky

* E-mail: liton.icosp@gmail.com

Way (see for instance Bilalbegović & Baranović 2015, and references therein). The most complex S-bearing molecule, ethyl mercaptan $\text{CH}_3\text{CH}_2\text{SH}$, was recently detected by Kolesníková et al. (2014) in Orion. Previously methyl mercaptan CH_3SH was first detected in SgrB2 (Linke et al. 1979) followed by observations in the organic-rich hot core G327.3-0.6 (Gibb et al. 2000b), and in Orion (Kolesníková et al. 2014). Gibb et al. (2000b) suggested that CH_3SH forms in the ices and then evaporates in hot cores. This paper reports the detection of CH_3SH in IRAS 16293-2422 followed by astrochemical modelling in order to explain the observed abundances. The observations and analysis are presented in Section 2. The chemical model is described in Section 3 while the results are discussed in the last Section.

2 OBSERVATIONS AND DATA REDUCTION

2.1 Observations

Observations were carried out using the IRAM 30m telescope from the 18th to the 23rd of August in average summer conditions (a median value of 4-6 mm water vapor). We used the EMIR heterodyne 3 mm receiver tuned at a frequency of 89.98 GHz in the Lower Inner sideband. The receiver was followed by a Fourier Transform Spectrometer in its 195 kHz resolution mode, the observed spectrum is composed of two approximately 8 GHz regions centered respectively on 88.41 and 104.06 GHz.

The beam size corresponding to the median value of the frequencies of the observed lines is $24.5''$ and this corresponds to 2940 AU for a distance of 120 pc (Crimier et al. 2010). The separation between source A and B is $5.5''$, so that both sources are well within the telescope beam. The position $\alpha_{2000} = 16^{\text{h}}32^{\text{m}}22.75^{\text{s}}$, $\delta_{2000} = -24^{\circ}28'34.2''$, midway between sources A and B of IRAS16293 was observed using the wobbler switching mode with a period of 2 seconds and a throw of $90''$ ensuring mostly flat baselines even in summer conditions and observations at low elevation. The nearby planet Saturn was used for focus (at the beginning of each run and after sunset) and pointing (every hour) with mostly good pointing corrections (less than a third of the beam size).

2.2 Results

2.2.1 CH_3SH line properties

We used the CLASS software from the GILDAS¹ package to reduce and analyse the data. Gaussian fits were made to the detected lines following a local low (0 or 1) order polynomial baseline subtraction. Table 1 and Fig. 1 show the result of these fits for the 6 observed lines of CH_3SH . Some observed lines correspond to unresolved spectral components, in these cases a single gaussian was fitted, which is often wider than the line corresponding to a single component, this is particularly important for lines 3 and 4, having spectral components separated by ~ 3 km/s. For the 3 single component features, the mean LSR velocity is 3.67 km s^{-1}

and the mean FWHM is 3.8 km s^{-1} . Caux et al. (2011) established a classification of the species in a FWHM vs VLSR plane, CH_3SH is similar to the cluster identified as Type IV not associated specifically to any of the two spatial components A or B of IRAS16293, these species either come from a common envelope or are found in the two components.

2.2.2 CH_3SH radiative transfer modelling

We use an LTE approach to model the emission of CH_3SH , the parameters in the radiative transfer model are the species column density, the line width, the excitation temperature and the source size (we assume an axisymmetric gaussian source centred in an axisymmetric gaussian beam whose size is dependent on the observed frequency). The model also requires accurate molecular spectroscopic data in the form of a catalog file which contains energy levels with associated quantum numbers, statistical weights and transition frequencies as well as the integrated intensity at 300 K. For CH_3SH , it was retrieved from the CDMS (Müller et al. 2005) using the VAMDC portal (Dubernet et al. 2010) and the frequencies, Einstein coefficients and upper level energies are listed in Table 1. When several lines of CH_3SH are blended in a single observed profile, we sum the corresponding modelled integrated intensities. This is appropriate in the low opacity regime observed for CH_3SH in IRAS16293.

We use a bayesian approach to recover the distribution of parameters which best agree with the observed line intensities. The likelihood is constructed assuming gaussian centred noise with a magnitude defined by the observed uncertainties on the observed integrated areas. The prior are chosen to be uniform and non informative over the range of variation as defined in Table 2, except for the line width for which a gaussian prior of mean 3.66 and standard deviation 0.2, corresponding to the median and typical errors of the single component gaussian line fits. This is done because in the optically thin regime where CH_3SH emits in IRAS16293, the integrated intensity is independent of the line width.

The posterior distribution function is sampled using the Affine Invariant Ensemble Monte Carlo Markov Chain approach described in Goodman & Weare (2010) in its Python implementation EMCEE² (Foreman-Mackey et al. 2013). One hundred walkers are initialised uniformly within the parameter ranges used and the chains are evolved for a burning sequence of 20000 steps after which the convergence is checked by examining a plot of the running mean of each parameters.

Figure 2 shows the 1D and 2D histogram of the posterior probability distribution function and the comparison of the observations with the distribution of computed intensities corresponding to the posterior distribution of parameters. Table 3 summarises the point estimates for the parameters. The H_2 column density is computed by integrating the power law in Crimier et al. (2010) up to the size derived by the bayesian method. The H_2 column density corresponding to the derived distribution of radius is $1.11 \pm 0.02 \times 10^{24} \text{ cm}^{-2}$, the uncertainties on the abundance will be dominated by the uncertainties on the CH_3SH column density. The distribution of line opacities of the observed line can also be determined from the posterior distribution of the parameters.

¹ <https://www.iram.fr/IRAMFR/GILDAS/>

² <https://github.com/dfm/emcee>

Table 1. Spectroscopic data for the observed lines of CH₃SH and derived line parameters.

Lines	W (K km s ⁻¹)	V _{LSR} (km s ⁻¹)	FWHM (km s ⁻¹)	Frequency (MHz)	A _{ij} (s ⁻¹)	E _{up} (K)	QNs
1	59.31 ± 5.01	3.6 ± 0.2	4.2 ± 0.4	101029.81	2.15 × 10 ⁻⁶	11.8	4 _{1,4} → 3 _{1,3} (E-)
2	122.05 ± 4.4	4.4 ± 0.7	3.8 ± 0.2	101139.16	2.31 × 10 ⁻⁶	7.3	4 _{0,4} → 3 _{0,3} (A+)
				101139.65	2.31 × 10 ⁻⁶	8.7	4 _{0,4} → 3 _{0,3} (E+)
3	49.01 ± 4.3	4.5 ± 0.3	6.9 ± 0.6	101159.46	1.73 × 10 ⁻⁶	26.4	4 _{2,3} → 3 _{2,2} (A-)
				101160.53	1.01 × 10 ⁻⁶	47.5	4 _{3,2} → 3 _{3,1} (E-)
				101160.53	1.01 × 10 ⁻⁶	47.7	4 _{3,2} → 3 _{3,1} (A+)
				101160.53	1.01 × 10 ⁻⁶	47.7	4 _{3,1} → 3 _{3,0} (A-)
4	53.70 ± 5.5	3.6 ± 0.3	6.3 ± 0.8	101167.15	1.73 × 10 ⁻⁶	24.8	4 _{2,3} → 3 _{2,2} (E-)
				101168.34	1.73 × 10 ⁻⁶	25.4	4 _{2,2} → 3 _{2,1} (E+)
5	40.90 ± 5.03	3.7 ± 0.2	2.9 ± 0.4	101284.36	2.17 × 10 ⁻⁶	13.5	4 _{1,3} → 3 _{1,2} (E+)
6	51.51 ± 3.62	3.7 ± 0.2	4.4 ± 0.4	102202.43	2.23 × 10 ⁻⁶	12.4	4 _{1,3} → 3 _{1,2} (A-)

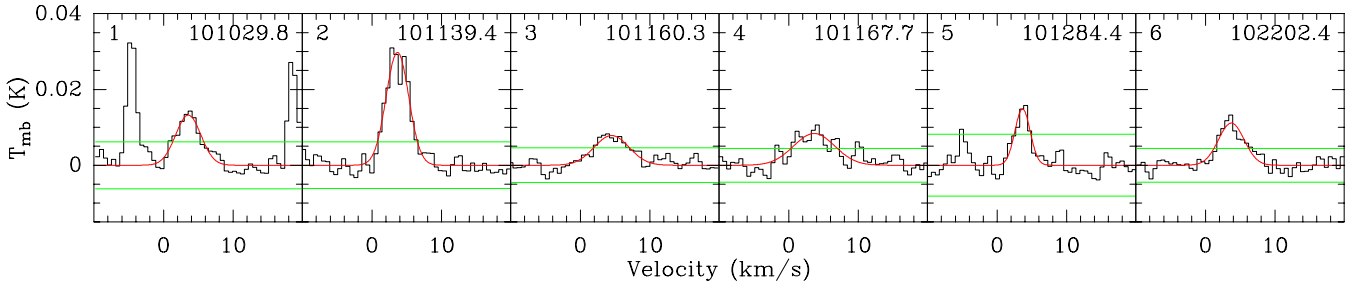


Figure 1. Gaussian fits to the observed line attributed to CH₃SH. The number in the top left of each panel corresponds to the line number in Table 1. The two additional lines in the first panel are H₂CCO lines. The green lines are ±3σ levels.

The derived line opacities range from 4×10^{-3} to 2×10^{-2} validating the optically thin hypothesis necessary to sum the blended line intensities.

It is not possible to infer the source size solely from the observed line intensities. As a matter of fact, we have observed the source in a limited range frequency and as a consequence, the different beam sizes are very close each other (only 1% relative variation). However, the range in upper level energies is large enough that the excitation temperature can be estimated accurately. By assuming LTE conditions, we have an estimate of the gas temperature of the region emitting in CH₃SH. Crimier et al. (2010) have determined the temperature and density profile of IRAS16293 as a function of radius. By using a parametrization of the gas temperature as a function of radius based on their Fig. 7, it is possible to attribute a source size for any given gas temperature. This estimated size can then be used to derive the overall beam dilution in the telescope beam and compute a column density corrected from the beam dilution. This reasoning is applied in a self coherent manner to determine all the model parameters from the dataset.

There remains the possibility that emission of CH₃SH coming from hotter gas in the more central parts of the pre-stellar envelope could also be detected and bias the measured parameters. It is possible to check that this contamination is negligible in our case. Indeed, emission from the inner hotter parts of the pre-stellar envelope at a temperature of 200 K (6 times larger than the 30 K computed) is associated with a

Table 2. Priors distribution functions for the parameters used in the bayesian approach.

Parameter	Distribution
log N	Uniform(9, 22)
T _{ex}	Uniform(3, 200)
ΔV	Normal(3.66, 0.2)

Notes: Uniform(min-value, max-value) is a uniform distribution with values going from minimum value to maximum value, Normal(μ , σ) is a gaussian distribution with mean μ and standard deviation σ

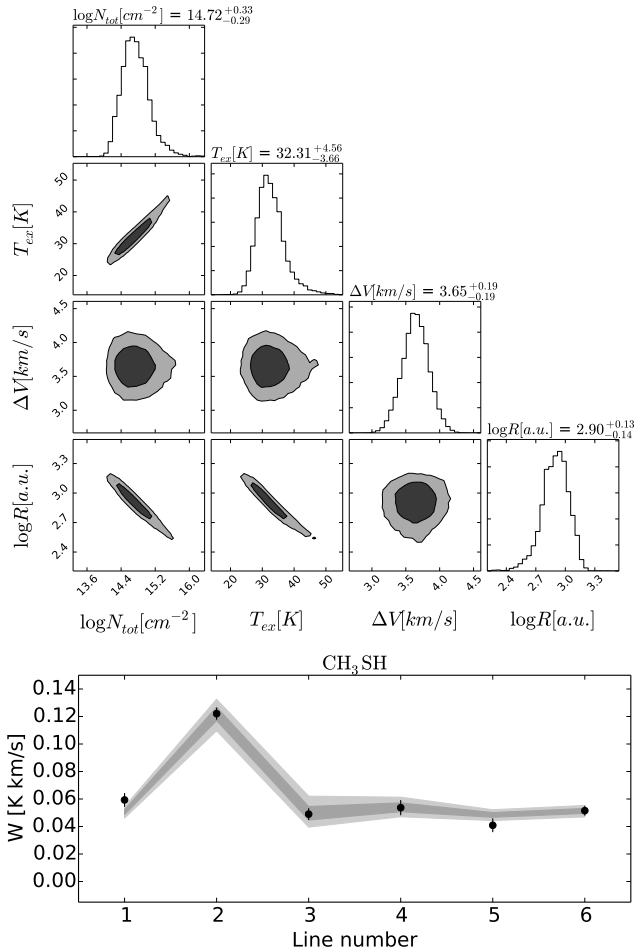
source size of only 10 AU (80 times smaller than the 760 AU computed). CH₃SH emission from the hotter central parts will be $80^2/6 \sim 1000$ times less bright than the detected emission. This is much lower than the detection limit. In terms of abundances towards the inner part, this translates into very high upper limits [CH₃SH] < 5×10^{-8} , the chemical modelling results showing a constant abundance of 4×10^{-9} for radii lower than 200 AU is thus compatible with the observations.

2.2.3 Validity of LTE

The LTE approach is only valid if the number density is much larger than the critical density of a given molecular transition. Using the density profile derived by Crimier et al. (2010), we find that the density of H₂ is of the order

Table 3. Point estimates of the posterior distribution function corresponding to the median and one sigma uncertainty.

Parameter	Value
$\log N(\text{CH}_3\text{SH})$ (cm^{-2})	14.7 ± 0.3
T_{ex} (K)	32 ± 4
ΔV (km s^{-1})	3.7 ± 0.2
$\log R$ (a.u.)	2.90 ± 0.13
$\log[\text{CH}_3\text{SH}]^a$	-9.3 ± 0.3

Notes: ^a $[X] = N(X)/N(\text{H}_2)$ **Figure 2.** 1D and 2D histograms of the posterior distribution of parameters. Contours contain respectively 68 and 95 percent of samples. Uncertainties are at the 16th and 84th percentile around the median value of the distribution. Bottom: observed integrated intensities and 1σ and 2σ distribution of the models corresponding to the posterior distribution of parameters. Lower axis indices correspond to the line numbers in Table 1.

of $3 \times 10^6 \text{ cm}^{-3}$. The collisional (de)excitation rates are not known for CH_3SH , however we can approximate their value to the ones of methanol or methylcyanide for similar transitions: $\sim 10^{-11} \text{ cm}^3 \text{ s}^{-1}$, with typical Einstein coefficients of $\sim 10^{-6} \text{ s}^{-1}$, this yields a critical density of $\sim 10^5 \text{ cm}^{-3}$, more than an order of magnitude below the H_2 density. Since the density of IRAS16293 is relatively high, we expect that

the abundances derived in the LTE approximation are only moderately underestimated. The similar type of approach was considered in the past for analysing Complex Organic Molecules (COMs) in IRAS16293 (Jaber et al. 2014).

3 CHEMICAL MODELING & NETWORK

3.1 The NAUTILUS chemical model

To simulate the abundance of CH_3SH in IRAS16293, the NAUTILUS gas-grain chemical model (Semenov et al. 2010; Reboussin et al. 2014) has been used with spherical protostellar core physical conditions similar to Aikawa et al. (2008, 2012). NAUTILUS is a state of the art chemical code which computes the abundances of species (e.g. atoms, ions, radicals, molecules) as a function of time in the gas phase and at the surface of the interstellar grains. All the equations and physicochemical processes included in the model were discussed in detail in Reboussin et al. (2014) and in Ruaud et al. (2015).

By following the kida.uva.2014 chemical network of Wakelam et al. (2015), several types of chemical reactions are considered in the gas phase. For example: bimolecular reactions between neutral species, between charged species and between neutral and charged species, unimolecular reactions i.e. photoreactions with direct UV photons and UV photons produced by the deexcitation of H_2 excited by cosmic ray particles, and direct ionisation and dissociation by cosmic ray particles. The grain surface is modeled by a one phase rate equation approach (Hasegawa et al. 1992), i.e. there is no differentiation between the species in the bulk and at the surface. The interactions of gas-phase species with the interstellar grains are considered via four major steps: physisorption of gas phase species onto grain surfaces, diffusion of the accreted species, reaction at the grain surface and finally by evaporation to the gas phase. Our model also considers different types of evaporation process such as thermal evaporation, evaporation induced by cosmic rays (following Hasegawa & Herbst 1993), and chemical desorption as suggested by Garrod et al. (2007). To simulate the chemistry of IRAS16293, we adopt the similar initial abundances reported in Hincelin et al. (2011), with an additional elemental abundance of 6.68×10^{-9} (compared to the total proton density) for fluorine (Neufeld et al. 2005) and a C/O elemental ratio of 0.7 (i.e. the oxygen elemental abundance is 2.4×10^{-4}).

3.2 Extension of the network

To follow the chemistry of CH_3SH , we have added several new reactions that are listed in Table A1. Most of the reactions in Table A1 are defined based on similarities with methanol and by following the well known reactivity of carbon atoms. For the reactions at the surface of the grains, we assume that CH_3SH forms through successive hydrogenation reactions of CS similarly to CH_3OH since quantum chemical calculations show that all the steps are exothermic in nature. Among all these added surface reactions, there are barriers for s-H + s-CS and s-H + s-H₂CS reactions but smaller than for s-H + s-CO and s-H + s-H₂CO reactions. This can be explained by the d-orbitals of sulphur. As for both oxygen and

sulphur, there is no occupied d orbital in the ground state so both 3d orbitals are vacant. But for sulphur, the energy needed to promote an electron from 3s or 3p orbital to 3d orbital is much less than the energy needed for an electron in the 2s or 2p orbitals in oxygen to 3d orbital. For this reason, the barrier we assumed for s-H+ s-H₂CS reaction is 1500 K. This value is close to the average of the calculated value at M06-2X/cc-pVTZ level (750 K) and MP2/cc-pVTZ level (2250K).

3.3 The Protostellar physical model

The chemistry of CH₃SH in IRAS 16293 is modeled using the same physical structure as in Aikawa et al. (2008) and Wakelam et al. (2014), and was computed using the radiation hydrodynamical (RHD) model from Masunaga & Inutsuka (2000). This model initially starts from a dense molecular cloud core with a central density $n(\text{H}_2) \sim 3 \times 10^4 \text{ cm}^{-3}$ and the core is extended up to $r = 4 \times 10^4 \text{ AU}$ with a total mass of $3.852 M_\odot$. The prestellar core evolves to the protostellar core in $2.5 \times 10^5 \text{ yr}$. When the protostar is formed, the model again follows the evolution for $9.3 \times 10^4 \text{ yr}$, during which the protostar grows by mass accretion from the envelope. Crimier et al. (2010) constrained the physical structure of the IRAS 16293 envelope through multi-wavelength dust and molecular observations. The physical structure of the envelope used for this study at the final time of the simulation is similar to Crimier et al. (2010).

4 MODELING RESULTS AND DISCUSSIONS

Figure 3 shows the computed abundances of CH₃SH, in the gas-phase and at the surface of the grains in the protostellar envelope as a function of radius to the central protostar. When the temperature increases above 30 K around 1000 AU, the gas-phase abundance of CH₃SH increases sharply up to 4×10^{-9} . The CH₃SH abundance on the grains shows an inverse profile showing that at low temperature, the CH₃SH molecule is formed on the grains (in the outer part of the envelope) and is thermally desorbed in the inner part of the envelope when the temperature exceeds the evaporation temperature of the species. Here our model results have been obtained assuming a depleted sulphur elemental abundance of 8×10^{-8} (compared to H₂) for both the pre-collapse and the protostellar phases. We also ran our model assuming that the missing sulphur is released into the gas-phase in atomic form in the hot corino with an abundance of 1×10^{-5} (compared to H₂). The gas-phase abundance of CH₃SH is 5×10^{-8} (compared to H₂) in that case. The CH₃SH abundance predicted by our model in the gas phase is thus compatible with the observations. Another parameter that may influence the CH₃SH gas-phase profile in the protostellar envelope is the assumed binding energy, which is not known. In our model, we assumed a binding energy of 2700 K, which results in an evaporation of this species around 500 AU from the central star, corresponding to a temperature around 50 K.

The identification of CH₃SH in a low mass protostar opens new opportunities to look for other complex sulphur bearing species. From Table A1, it is clear that H₂CS, CH₃S are some of the species related to the formation of CH₃SH. According to Vandeputte et al. (2010), reaction between

CH₃SH and CH₃S, H₂CS can lead to (CH₃S)₂. Cruz-Torres et al. (2007) has also shown that reaction between CH₃SH and OH can lead to CH₃SOH. Spectroscopic data for these species are however missing for the moment.

ACKNOWLEDGEMENTS

Based on observations carried out with the IRAM 30m Telescope. IRAM is supported by INSU/CNRS (France), MPG (Germany) and IGN (Spain). LM, PG, VW and TV thanks ERC starting grant (3DICE, grant agreement 336474) for funding during this work. PG postdoctoral position is funded by the INSU/CNRS. VW, JCL and KMH acknowledge the CNRS programme PCMI for funding of their research. We also thank the anonymous reviewer for his useful comments to improve the manuscript.

REFERENCES

- Aikawa Y., Wakelam V., Garrod R. T., Herbst E., 2008, *ApJ*, **674**, 984
Aikawa Y., Wakelam V., Hersant F., Garrod R. T., Herbst E., 2012, *ApJ*, **760**, 40
Anderson D. E., Bergin E. A., Maret S., Wakelam V., 2013, *ApJ*, **779**, 141
Anicich V. G., 1993, *Journal of Physical and Chemical Reference Data*, **22**, 1469
Bilalbegović G., Baranović G., 2015, *MNRAS*, **446**, 3118
Boogert A. C. A., Tielens A. G. G. M., Ceccarelli C., Boonman A. M. S., van Dishoeck E. F., Keane J. V., Whittett D. C. B., de Graauw T., 2000, *A&A*, **360**, 683
Buckle J. V., Fuller G. A., 2003, *A&A*, **399**, 567
ButkovskayaĀĀ N. I., D. W. Setser* Ā., 1999, *The Journal of Physical Chemistry A*, **103**, 6921
Caux E., et al., 2011, *A&A*, **532**, A23
Charnley S. B., 1997, *ApJ*, **481**, 396
Crimier N., Ceccarelli C., Maret S., Bottinelli S., Caux E., Kahane C., Lis D. C., Olofsson J., 2010, *A&A*, **519**, A65
Cruz-Torres A., Galano* A., 2007, *The Journal of Physical Chemistry A*, **111**, 1523
DeckerĀĀ B. K., Macdonald* R. G., 2001, *The Journal of Physical Chemistry A*, **105**, 6817
Dobe S., Berces T., Szilagyi I., 1991, *J. Chem. Soc., Faraday Trans.*, **87**, 2331
Druard C., Wakelam V., 2012, *MNRAS*, **426**, 354
Dubernet M. L., et al., 2010, *J. Quant. Spectrosc. Radiative Transfer*, **111**, 2151
Ewig F., RhĀĀ'sa D., Zellner R., 1987, *Berichte der Bunsengesellschaft fĀĀjr physikalische Chemie*, **91**, 708
Foreman-Mackey D., Hogg D. W., Lang D., Goodman J., 2013, *PASP*, **125**, 306
Garrod R. T., Wakelam V., Herbst E., 2007, *A&A*, **467**, 1103
Geppert W. D., et al., 2006, *Faraday Discussions*, **133**, 177
Gibb E. L., et al., 2000a, *ApJ*, **536**, 347
Gibb E., Nummelin A., Irvine W. M., Whittett D. C. B., Bergman P., 2000b, *ApJ*, **545**, 309
Goodman J., Weare J., 2010, *Commun. Appl. Math. Comput. Sci.*, **5**
Hasegawa T. I., Herbst E., 1993, *MNRAS*, **261**, 83
Hasegawa T. I., Herbst E., Leung C. M., 1992, *ApJS*, **82**, 167
Hatchell J., Thompson M. A., Millar T. J., MacDonald G. H., 1998, *A&A*, **338**, 713
Hincelin U., Wakelam V., Hersant F., Guilloteau S., Loison J. C., Honvault P., Troe J., 2011, *A&A*, **530**, A61

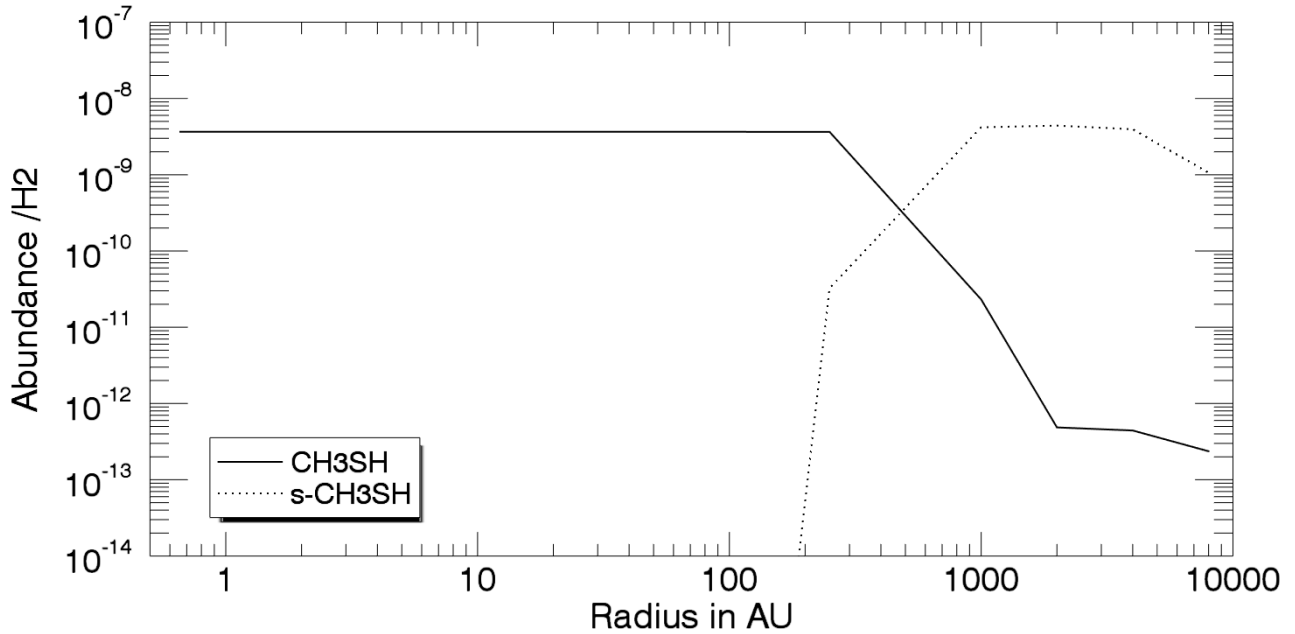


Figure 3. CH₃SH abundance (with respect to H₂) predicted by our model as a function of radius. s-CH₃SH represents the CH₃SH on the surface of grains.

1981, *Symposium (International) on Combustion*, 18, 831

Hynes A. J., Wine P. H., 1987, *The Journal of Physical Chemistry*, 91, 3672

Jaber A. A., Ceccarelli C., Kahane C., Caux E., 2014, *ApJ*, 791, 29

Jenkins E. B., 2009, *ApJ*, 700, 1299

Kolesniková L., Tercero B., Cernicharo J., Alonso J. L., Daly A. M., Gordon B. P., Shipman S. T., 2014, *ApJ*, 784, L7

Li J., Wang J., Zhu Q., Zhang J., Li D., 2015, *ApJ*, 802, 40

Linke R. A., Frerking M. A., Thaddeus P., 1979, *ApJ*, 234, L139

Masunaga H., Inutsuka S.-i., 2000, *ApJ*, 531, 350

Millar T., 1982, *Astrophysics and Space Science*, 87, 435

Müller H. S. P., Schlöder F., Stutzki J., Winnewisser G., 2005, *Journal of Molecular Structure*, 742, 215

Neufeld D. A., Wolfire M. G., Schilke P., 2005, *ApJ*, 628, 260

Penzias A. A., Solomon P. M., Wilson R. W., Jefferts K. B., 1971, *ApJ*, 168, L53

Reboussin L., Wakelam V., Guilloteau S., Hersant F., 2014, *MNRAS*, 440, 3557

Ruaud M., Loison J. C., Hickson K. M., Gratier P., Hersant F., Wakelam V., 2015, *MNRAS*, 447, 4004

Semenov D., et al., 2010, *A&A*, 522, A42

Shannon R. J., Cossou C., Loison J.-C., Caubet P., Balucani N., Seakins P. W., Wakelam V., Hickson K. M., 2014, *RSC Adv.*, 4, 26342

Sofia U. J., Cardelli J. A., Savage B. D., 1994, *ApJ*, 430, 650

Tieftrunk A., Pineau des Forets G., Schilke P., Walmsley C. M., 1994, *A&A*, 289, 579

Vandeputte A. G., Reyniers M.-F., Marin G. B., 2010, *The Journal of Physical Chemistry A*, 114, 10531

Wakelam V., Castets A., Ceccarelli C., Lefloch B., Caux E., Paganani L., 2004a, *A&A*, 413, 609

Wakelam V., Caselli P., Ceccarelli C., Herbst E., Castets A., 2004b, *A&A*, 422, 159

Wakelam V., Hersant F., Herpin F., 2011, *A&A*, 529, A112

Wakelam V., Vastel C., Aikawa Y., Coutens A., Bottinelli S., Caux E., 2014, *MNRAS*, 445, 2854

Wakelam V., et al., 2015, *ApJS*, 217, 20

Woods P. M., Occhiogrosso A., Viti S., Kaňuchová Z., Palumbo M. E., Price S. D., 2015, *MNRAS*, 450, 1256

van Dishoeck E. F., Blake G. A., 1998, *ARA&A*, 36, 317

APPENDIX A: LIST OF ADDED REACTIONS

This paper has been typeset from a T_EX/L^AT_EX file prepared by the author.

Table A1. List of gas-phase and grain surface reactions added to the model and associated parameters.

	Reaction		α	β	γ	Reference
1	H + CH ₃ S	→ H ₂ CS + H ₂	3.00×10^{-11}	0	0	2
		→ CH ₃ + HS	3.00×10^{-12}	0	0	2
2	S + CH ₃ S	→ H ₂ CS + HS	6.00×10^{-12}	0	0	9
		→ CH ₃ + S ₂	1.90×10^{-11}	0	0	9
3	C + CH ₃ S	→ CH ₃ + CS	3.00×10^{-10}	0	0	3
4	N + CH ₃ S	→ H ₂ CS + NH	1.00×10^{-11}	-0.17	0	9
		→ CH ₃ + NS	6.00×10^{-11}	0	0	9
5	O + CH ₃ S	→ CH ₃ + SO	4.00×10^{-11}	0	0	5
6	C + CH ₃ SH	→ CH ₃ + HCS	3.00×10^{-10}	0	0	4
7	CN + CH ₃ SH	→ CH ₃ S + HCN	2.70×10^{-10}	0	0	7
8	OH + CH ₃ SH	→ CH ₃ S + H ₂ O	8.00×10^{-12}	-0.4	0	6
9	H ₂ S + CH ₃ ⁺	→ CH ₃ SH ₂ ⁺ + Photon	2.00×10^{-9}	0	0	10
10	CH ₃ SH + He ⁺	→ CH ₃ ⁺ + He + HS	0.5	2.82×10^{-9}	3.32	1
11	CH ₃ SH + H ₃ ⁺	→ CH ₃ SH ₂ ⁺ + H ₂	3.20×10^{-9}	2.3	3	1
12	CH ₃ SH + CH ₄ ⁺	→ CH ₃ SH ₂ ⁺ + CH ₃	0.40	1.56×10^{-9}	3.32	1
		→ CH ₃ SH ⁺ + CH ₄	0.6	1.56×10^{-9}	3.32	1
13	CH ₃ SH + C ⁺	→ CH ₃ ⁺ + HCS	0.80	1.75×10^{-9}	2.33	1
		→ CH ₃ S ⁺ + CH	0.20	1.75×10^{-9}	2.33	1
14	CH ₃ SH + HCO ⁺	→ CH ₃ SH ₂ ⁺ + CO	1.30×10^{-9}	2.3	3	1
15	CH ₃ SH + N ⁺	→ CH ₃ + H + NS ⁺	0.1	1.64×10^{-9}	3.32	1
		→ CH ₃ ⁺ + H + NS	0.04	1.64×10^{-9}	3.32	1
		→ H ₂ CS ⁺ + H + NH	0.3	1.64×10^{-9}	3.32	1
		→ CH ₃ SH ⁺ + N	0.4	1.64×10^{-9}	3.32	1
16	CH ₃ SH + O ⁺	→ H ₂ CS ⁺ + H ₂ O	0.05	1.56×10^{-9}	3.32	1
		→ CH ₃ SH ⁺ + O	0.25	1.56×10^{-9}	3.32	1
17	CH ₃ SH + H ₃ O ⁺	→ CH ₃ SH ₂ ⁺ + H ₂ O	1.50×10^{-9}	2.3	3	1
18	CH ₃ SH + CH ⁺	→ CH ₃ SH ₂ ⁺ + C	0.4	1.70×10^{-9}	3.32	1
		→ H ₂ CS + CH ₃ ⁺	0.5	1.70×10^{-9}	3.32	1
19	CH ₃ SH + O ₂ ⁺	→ CH ₃ SH ⁺ + O ₂	0.5	1.23×10^{-9}	3.32	1
20	CH ₃ SH + H ⁺	→ CH ₃ SH ⁺ + H	0.5	5.5×10^{-9}	3.32	1
		→ CH ₃ ⁺ + H ₂ S	0.25	5.5×10^{-9}	2.3	1
		→ HCS ⁺ + H ₂ + H ₂	0.25	5.5×10^{-9}	2.3	1
21	CH ₃ SH + Photon	→ H ₂ CS + H ₂	1.40×10^{-9}	0	2.28	9
		→ CH ₃ SH ⁺ + e ⁻	7.00×10^{-10}	0	2.57	9
		→ HS + CH ₃	1.20×10^{-9}	0	2.28	9
22	CH ₃ SH + CRP	→ H ₂ CS + H ₂	3.17×10^3	0	0	9
		→ CH ₃ SH ⁺ + e ⁻	1.44×10^3	0	0	9
		→ HS + CH ₃	1.50×10^3	0	0	9
23	CH ₃ SH ⁺ + e ⁻	→ HS + CH ₃	3.00×10^{-7}	-0.5	0	9
		→ H ₂ + H ₂ CS	3.00×10^{-7}	-0.5	0	9
24	CH ₃ SH ₂ ⁺ + e ⁻	→ H ₂ S + CH ₃	8.00×10^{-8}	-0.59	0	8
		→ H + H ₂ CS + H ₂	5.90×10^{-8}	-0.59	0	8
		→ H + CH ₃ + HS	4.50×10^{-7}	-0.59	0	8
		→ H + CH ₂ + H ₂ S	1.90×10^{-7}	-0.59	0	8
		→ H + CH ₃ SH	2.70×10^{-8}	-0.59	0	8
		→ H ₂ + CH ₃ S	5.30×10^{-8}	-0.59	0	8
1	s-H + s-CS	→ s-HCS	1	0	0	9
2	s-H + s-CH ₃ S	→ s-CH ₃ SH	1	0	0	9
3	s-H + s-H ₂ CS	→ s-CH ₃ S	1	0	0	9
4	s-S + s-CH ₃	→ s-CH ₃ S	1	0	0	9

1 Rate constant calculated considering capture theory (using $\mu = 1.56$ Debye and $\alpha = 5.4$ Angstrom). Good agreement with (Anicich 1993), branching ratio assumed from (Anicich 1993).
 2 Following H + CH₃O reaction from (Hoy 1981; Dobe et al. 1991)
 3 Considering the various C reactions.
 4 Following C + CH₃OH reaction from (Shannon et al. 2014)
 5 Following O + CH₃O reaction from (Ewig et al. 1987)
 6 Following (Hynes & Wine 1987; Butkovskaya et al. 1999)
 MNRAS 000, 000–000 (2015) Following (Decker et al. 2001), branching ratio guessed from the OH + CH₃O reaction
 8 Following (Geppert et al. 2006)
 9 Following the similar reactions of CH₃OH and its related species
 10 Following (Millar 1982)